JOURNAL OF SOLID STATE CHEMISTRY 118, 20–27 (1995)

Pressure-Induced Phase Transition in $CsGeBr_3$ Studied by X-Ray Diffraction and Raman Spectroscopy

U. Schwarz,[1] H. Hillebrecht, M. Kaupp, K. Syassen, and H.-G. von Schnering

Max-Planck-Institut für Festkörperforschung, Heisenbergstrasse 1, D-70569 Stuttgart Germany

and

G. Thiele

Institut für Anorganische Chemie, Albertstrasse 21, D-79104 Freiburg, Germany

Received November 28, 1994; accepted January 9, 1995

We have investigated the effect of hydrostatic pressure on the structural properties of $CsGeBr_3$ by means of X-ray diffraction and Raman spectroscopy. Pressures were generated using diamond anvil cells. At 1.0(2) GPa the trigonal ambient pressure modification of $CsGeBr_3$ undergoes a reversible first-order phase transition to a high-pressure polymorph crystallizing in the cubic perovskite structure. The variation in Ge–Br bond length is obtained from single-crystal structure refinements of both the low- and the high-pressure modifications. The phase transformation occurs at a relative volume of $V/V_0 = 0.92$, and the prediction from Hartree–Fock calculations is in agreement with this experimental result. © 1995 Academic Press, Inc.

INTRODUCTION

ABX_3 compounds crystallizing in perovskite-like structures show a manifold of closely related structural variants. The cubic primitive crystal structure (aristotype) is often slightly distorted and the loss of symmetry can be described using group–subgroup relations (1, 2). Distortive phase transitions (3) causing small changes in crystal structures are frequently accompanied by pronounced changes in dielectric properties (4, 5). Perovskite-related phases containing atoms with an ns^2 electron configuration exhibit a particularly interesting structural chemistry. In a molecular picture, the electron density of an inert *s*-electron pair has inversion symmetry. The admixture of *p*-character usually results in a non-centrosymmetric electron density. The inert electron pair becomes stereochemically active and causes pronounced anisotropy in the coordination polyhedron of the atom with lone pair configuration.

Cesium trihalogenometallates(II) $CsMX_3$ of group 14 elements (M = Ge, Sn, Pb; X = Cl, Br, I) contain ns^2 cations M(II) and crystallize in perovskite variants with lower symmetry under ambient conditions. In particular the germanium compounds can serve as model substances for investigating physical properties and phase transitions, since untwinned single crystals of the non-centrosymmetric low-temperature modifications can be grown from aqueous solutions (6). Under ambient conditions $CsGeBr_3$ crystallizes in space group $R3m$ (No. 160) with a = 788.1 pm, c = 997.2 pm (7) (c is the polar axis in trigonal setting) and a_R = 536.5 pm, $\alpha = 88.74°$ (rhombohedral setting). Figure 1a shows a unit cell of the crystal structure under ambient conditions in the rhombohedral setting. Cesium and bromine together form a slightly distorted cubic closest packing. Germanium atoms are located in the nearly regular octahedral voids (trigonal antiprisms) formed by six bromine atoms, but shifted from the center toward one face of the coordination polyhedron. Thus, a trigonal antiprismatic (3 + 3)-coordination results with three shorter and three longer bonds d(Ge–Br): 253.4(3) pm and 311.6(4) pm (7). The coordination of Ge(II) is best described as Ψ-tetrahedral.

Temperature-dependent X-ray powder diffraction experiments (7) have revealed that $CsGeBr_3$ undergoes a phase transition to a high-temperature (HT) modification with cubic metric at 510 K. However, Raman spectra of the HT modification show basically the same modes as the low-temperature (LT) modification. Since no Raman-active modes are expected for the cubic primitive aristotype (space group $Pm\bar{3}m$) it was concluded that the cubic metric is caused by an order–disorder phase transition and that the local C_{3v} symmetry of the Ge(II) coordination

[1] To whom correspondence should be addressed.

0022-4596/95 $12.00

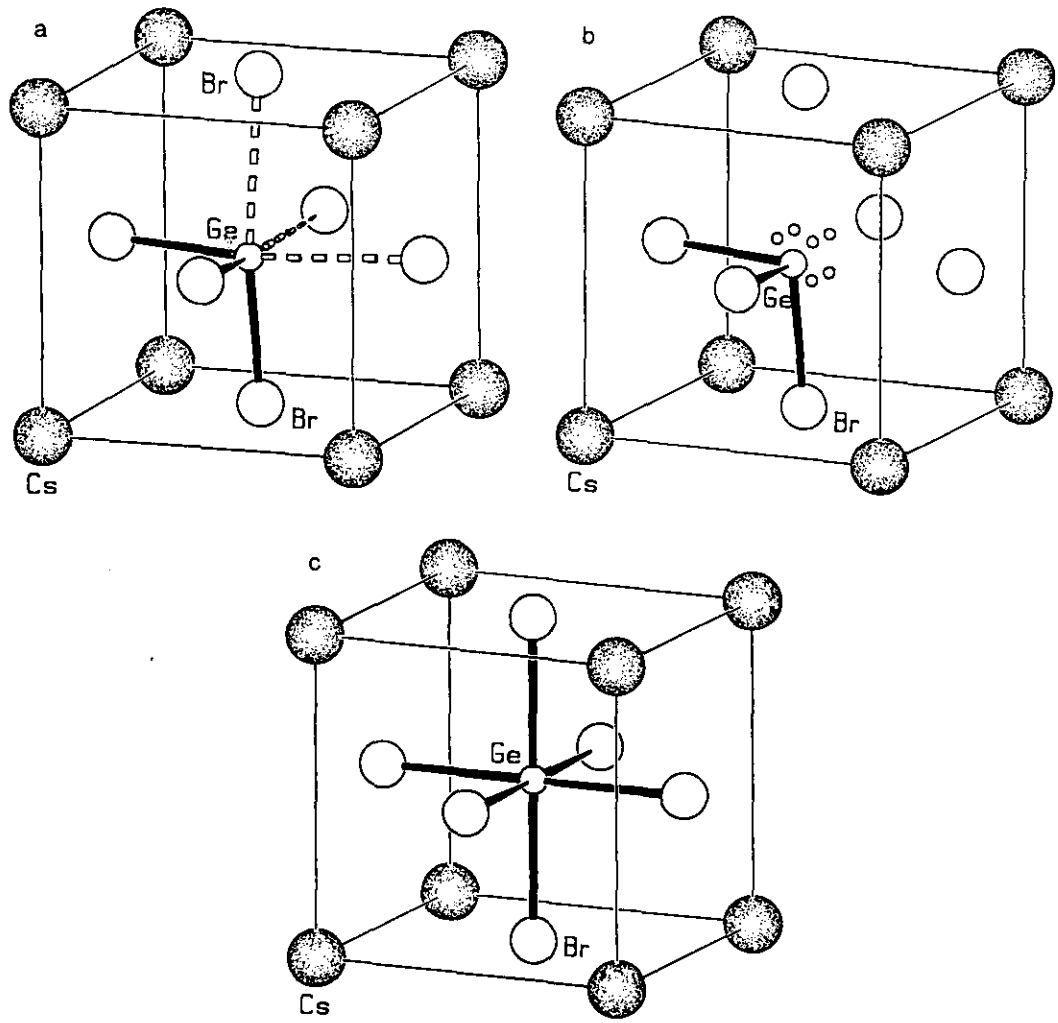

FIG. 1. Rhombohedral and cubic unit cells of $CsGeBr_3$ (origin front left): (a) under ambient conditions; (b) high-temperature modification above 513 K at 0.1 MPa (ambient pressure) with equivalent disorder positions of Ge indicated by small circles; (c) high-pressure modification above 1 GPa at ambient temperature.

polyhedra remains unchanged. Figure 1b shows the crystal structure of the HT polymorph, which is consistent with experimental observations (7).

The stereochemical activity of nonbonding valence electron pairs decreases with increasing atomic number (8). According to an empirical rule (9), high pressure causes phase transitions to crystal structures of heavier group homologues. Thus, we may expect that external pressure induces structural changes in $CsGeBr_3$, which result in less distorted coordination polyhedra of germanium.

We report here a high-pressure investigation of the structural properties of $CsGeBr_3$. X-ray diffraction experiments were performed to determine lattice parameters, volumes, and crystal structure under pressure. We have also used Raman spectroscopy as a method to obtain information on changes in local symmetry. The main reason is the usual high pseudosymmetry of perovskite-like crystal structures. Furthermore, it is a sensitive tool for distinguishing between distortive and order–disorder phase transitions. The X-ray diffraction experiments show that within the stability range of the ambient pressure polymorph, increasing pressure reduces both the deviation from a cubic metric and the 3 + 3 splitting of the Ge–Br distances. X-ray and Raman measurements consistently indicate a phase transition at 1.0(2) GPa to a high-pressure modification with a cubic primitive unit cell. Thus, we conclude that the crystal structure of this high-pressure polymorph is the cubic primitive perovskite (aristotype), which is shown in Fig. 1c.

EXPERIMENTAL

Yellow crystals of $CsGeBr_3$ were synthesized by dissolving $Ge(OH)_2$ in 4 *N* HBr and adding an excess of CsBr

(7). High pressures for Raman and X-ray diffraction measurements were generated using diamond anvil cells with prepressed Inconel gaskets of 0.1 mm thickness and holes of 0.25 mm diameter. Paraffin was used as a pressure-transmitting medium. Pressures were determined by the ruby luminescence method (10). Raman spectra were measured in near back-scattering set up using two different laser lines (Ar laser: 514.5 nm, Kr laser: 647.1 nm). The excitation power at the sample was kept below 2 mW in order to avoid local heating in the laser focus of about 0.1 mm diameter. The scattered light was dispersed by a triple-grating spectrometer and recorded with a multichannel detection system. X-ray powder diffraction patterns were measured in transmission mode with Zr-filtered radiation from a Mo tube or monochromatized and focused Mo$K\alpha_1$ radiation and a position-sensitive detection system. Intensities for crystal structure determinations were collected on a four-circle diffractometer, using a graphite monochromator and Mo$K\alpha$ radiation. Single crystal diffraction experiments were performed with a lightweight (200 g) Merril–Bassett-type pressure cell (11).

RESULTS

Raman Scattering

The first evidence for a pressure-induced phase transition in $CsGeBr_3$ was observed in Raman scattering experiments. Raman spectra of $CsGeBr_3$ at selected pressures are shown in Fig. 2. In accordance with previous results (7), six Raman lines are observed under ambient conditions.

The mode assignment shown in Fig. 3 is based on polarized Raman measurements for homologous compounds (12). For the displacement patterns of these modes we refer to Ref. (13). The pressure dependence of the mode frequencies is shown in Fig. 3. The dominant bands shift

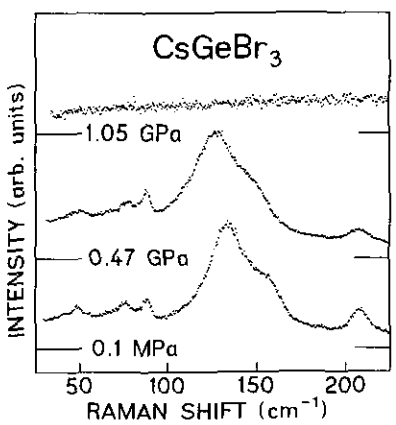

FIG. 2. Experimental Raman spectra at different pressures. The laser excitation wavelength is 647 nm.

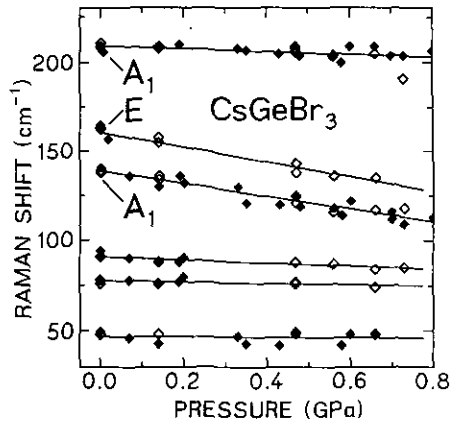

FIG. 3. Frequencies of Raman modes up to 0.8 GPa. The zero pressure frequencies ν_0 and the linear shifts $\Delta\nu/\Delta p$ corresponding to the solid lines are shown in Table 1. Excitation wavelengths: Open symbols: 647 nm; filled symbols: 514 nm.

to lower frequency with increasing pressure. For all lines these shifts are essentially linear between 0.1 MPa (ambient pressure) and 0.8 GPa. The corresponding pressure coefficients are listed in Table 1.

The Raman lines of the rhombohedral modification vanish completely at 1.0(2) GPa. For decreasing pressure, these Raman lines reappear at 0.7(1) GPa. We attribute the change in Raman spectra near 1 GPa to a reversible phase transition into a high pressure modification. The disappearance of Raman intensity indicates cubic symmetry and regular octahedral coordination of the Ge atoms. Raman spectra of the high-pressure modification measured with relatively high laser power (20 mW, green Ar line) show only a broad but weak Raman band with a maximum at approximately 100(5) cm^{-1}. This weak band is attributed to defect-induced scattering.

X-Ray Diffraction

X-ray powder diagrams of the low-pressure modification of $CsGeBr_3$ show a pattern of line splittings which is characteristic for trigonally distorted perovskites. At

TABLE 1

Assignments, Zero Pressure Frequencies ν_0, and Linear Shifts $\Delta\nu/\Delta p$ of the Raman Active Modes of $CsGeBr_3$

Assignment (12)	ν_0 (cm^{-1})	$\Delta\nu/\Delta p$ (cm^{-1}/GPa)
	47(1)	−1(3)
	77.5(5)	−3(2)
	91(1)	−8(2)
A_1	139(2)	−36(2)
E	161(2)	−42(5)
A_1	209(1)	−8(2)

pressures above 1.0(2) GPa the line splittings disappear for reflections within our observable 2Θ-range (<25°). Diagrams measured using monochromatic Mo$K\alpha_1$ radiation in a focusing setup with peaks of a typical full width at half-maximum of 0.1° give no indication of splitting or broadening, thus confirming the cubic metric of the high-pressure modification.

Line positions in the diffraction diagrams of both the low- and high-pressure modification were determined by least-squares fits of pseudo-Voigt peak shapes to the measured intensities. The *d*-values of about 10 reflections were measured for the low-pressure phase (trigonal *hkl*): (012), (110), (003), (021), (202), (21$\bar{2}$), (300), (024), (220), and (042). Using the program AGL (*14*), lattice constants of the unit cells in the trigonal setting were refined and finally transformed into rhombohedral lattice parameters. The pressure-induced increase in the rhombohedral angle α and the decrease in the Br–Ge–Br bond angle β are shown in Fig. 4. Near 1 GPa α and β change discontinuously to 90°. In Fig. 5 we show the pressure–volume relations for both the low- and high-pressure modifications. Within experimental accuracy, no discontinuous change in volume is observed at the phase transition. Zero pressure volumes V_0, bulk moduli B_0, and their pressure derivatives B_0' were determined by fitting a Murnaghan equation of state to the experimental data:

$$V(P) = V_0\left(\frac{PB_0'}{B_0} + 1\right)^{-1/B_0'}. \qquad [1]$$

The corresponding parameter values are given in the caption of Fig. 5.

Single-crystal structure refinements were carried out with two different crystals at four different pressures using

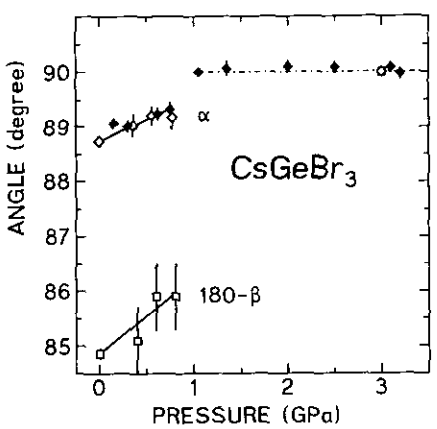

FIG. 4. Rhombohedral angle α and Br–Ge–Br bonding angle β of $CsGeBr_3$ up to 3.0 GPa. The solid line represents a linear least-squares fit to the experimental data. The dotted line at $\alpha = \beta = 90°$ is a visual guide. Open symbols: Single-crystal data; Filled symbols: Powder diffraction data.

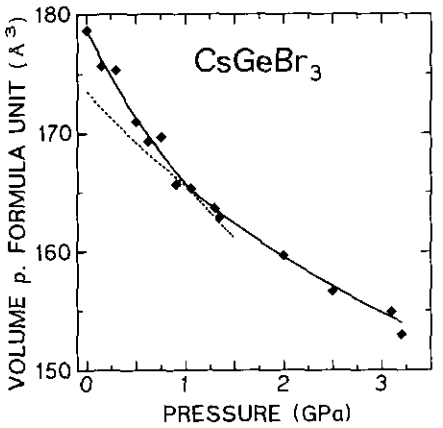

FIG. 5. Pressure–volume relation of $CsGeBr_3$. The solid lines correspond to least-squares fits of Murnaghan-type functions to the experimental data. Parameters describing the pressure–volume relations are: V_0 = 179(1) × 10^6 pm^3, B_0 = 11(1) GPa with B' = 6(2) (low-pressure modification) and V_0 = 174(1) × 10^6 pm^3, B_0 = 18(1) GPa with fixed B' = 6 (high-pressure modification). Dotted lines represent extrapolations into stability fields of other polymorphs.

the previously determined $V(P)$ relation as a pressure calibration. After raising the pressure carefully through the first-order phase transition regime it was possible to measure single-crystal diffraction intensities for the high-pressure phase. Crystal structure parameters were refined using the program SHELX76 (*15*).

The resulting positional and displacement parameters are given in Table 2. The small overall increase in displacement parameters from 0.1 MPa to 0.4 GPa may be attributed to X-ray absorption in the diamond anvil cell. The path for a diffracted beam through the diamond and the beryllium backing plate increases with diffraction angle, and the intensity loss due to absorption becomes more severe. Absorption reduces intensities with increasing diffraction angle in a way which is similar to the effect of

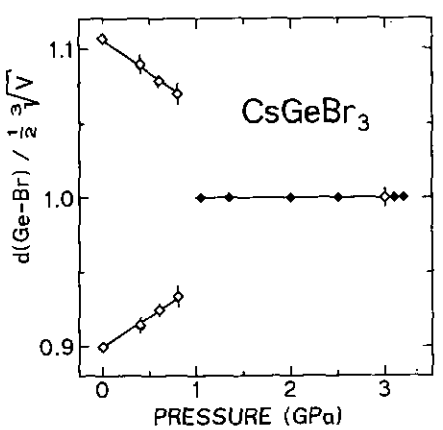

FIG. 6. Normalized distances d(Ge–Br)/$\frac{1}{2}\sqrt[3]{V}$ at various pressures up to 3.0 GPa. Open symbols: Single-crystal data; filled symbols: Powder data.

TABLE 2
Positional and Displacement Parameters (pm^2) of $CsGeBr_3$ at Pressures up to 3.0 GPa

Pressure (GPa)		0.0001	0.4	0.6	0.8	3.0
Remark		Data Ref. (7)	Crystal I	Crystal II	Crystal I	Crystal I
SG		$R3m$	$R3m$	$R3m$	$R3m$	$Pm\bar{3}m$
Cs	U_{11}	550(10)	608(23)	502(21)	466(23)	352(9)
	U_{12}	28(8)	196(26)	132(23)	118(26)	0
Ge	x	0.4764(4)	0.481(2)	0.482(2)	0.486(2)	½
	U_{11}	221(8)	296(25)	314(23)	190(25)	118(9)
	U_{12}	−1(6)	110(27)	152(26)	37(28)	0
Br	x	0.5018(4)	0.504(1)	0.502(2)	.506(2)	½
	z	0.0271(4)	0.026(1)	0.023(1)	.020(2)	0
	U_{11}	672(8)	782(23)	552(21)	548(24)	407(12)
	U_{33}	210(10)	200(25)	186(23)	216(27)	261(17)
	U_{12}	−10(6)	159(20)	50(19)	73(22)	0
	U_{23}	50(10)	238(25)	87(23)	116(26)	0

Note. Atomic positions in $R3m$: Cs at 1*a* (x, x, x) with $x = 0$, Ge at 1*a*, and Br at 3*b* (x, x, z); positions in $Pm\bar{3}m$: Cs at 1*a* (0, 0, 0), Ge at 1*b* (½, ½, ½), and Br at 3*c* (½, ½, 0).

an increased Debye–Waller factor. Thus, we expect larger displacement parameters in the subsequent refinement procedures. Nevertheless, the *R*-values and the displacement parameters (see Tables 2 and 3) prove the quality of the intensities measured at high pressures to be sufficient for reliable parameter refinements.

Important interatomic distances and angles are listed in Table 4. The pressure dependences of the normalized Ge–Br distances are shown in Fig. 6. In the low-pressure modification the shorter bond length *d*(Ge–Br) becomes slightly *larger* with increasing pressure, whereas the three longer distances *d'*(Ge–Br) decrease. The results of the single-crystal structure determination at 3.0 GPa (see Table 4) show no evidence for a deviation in the crystal structure from the cubic aristotype. Thus, single-crystal diffraction confirms that the coordination polyhedron of Ge(II) has changed into a regular octahedron (16).

Structural Calculations

In order to gain further insight into the structural behavior of $CsGeBr_3$ under pressure, Hartree–Fock (HF) calculations with periodic boundary conditions have been performed using the Crystal 92 program (17). Structural parameters have been optimized by pointwise successive variation. Two different pseudopotential/GTO (Gaussian-type orbitals) valence basis set combinations were used: (i) For the full optimization of all degrees of freedom for

TABLE 3
Data Collection and Refinement Parameters of $CsGeBr_3$ for Measurements at Pressures up to 3.0 GPa

Pressure (GPa)	0.0001	0.4	0.6	0.8	3.0
Remarks	Data Ref. (7)	Crystal I	Crystal II	Crystal I	Crystal I
Space group	$R3m$	$R3m$	$R3m$	$R3m$	$Pm\bar{3}m$
a (pm)	563.5(9)	558(2)	554(2)	551(2)	536(2)
α (°)	88.74(4)	89.0(1)	89.2(1)	89.2(1)	90
$V(10^6\ pm^3)$	178.6	173.4	170.3	167.1	154.3
Z	1	1	1	1	1
Θ/Range (°Θ)	1–24	1–30	1–35	1–30	1–30
Scan width (°)	0.7	1.05	1.05	1.05	1.35
Measured reflections	1238	623	616	592	545
Independent reflections	140	97	134	92	54
Refined variables	13	13	12	13	6
$\Delta\rho$ max. ($e^-/10^4\ pm^3$)		1.67	1.60	1.19	1.79
R value	0.037	0.060	0.079	0.062	0.063
R_w value	0.026	0.042	0.060	0.063	0.059

TABLE 4
Important Interatomic Distances (pm) and Bond Angles (°) in $CsGeBr_3$ from Single-Crystal Structure Determinations at Various Pressures

Pressure (GPa)	0.0001	0.4	0.6	0.8	3.0
Remarks	Data Ref. (7)	Crystal I	Crystal II	Crystal I	Crystal I
Space group	*R3m*	*R3m*	*R3m*	*R3m*	$Pm\bar{3}m$
d(Ge–Br)	253.4(3)	253(1)	256(1)	257(1)	268(2)
d'(Ge–Br)	311.6(4)	306(1)	299(1)	295(1)	
	394.3(3)	391(1)	389(1)	387(1)	
d(Cs–Br)	401.2(3)	394(1)	393(1)	387(1)	379(2)
	405.0(3)	402(1)	397(1)	397(1)	
	374.1(4)	374(1)	375(1)	376(1)	
d(Br–Br)	403.3(4)	398(1)	395(1)	392(1)	379(1)
	414.0(1)	409(1)	403(1)	397(1)	
Angle					
Br–Ge–Br	95.16(9)	94.9(6)	94.1(6)	94.1(9)	90

both the low- and high-pressure modification we used a 1-valence-electron pseudopotential (18) and a (3*s*2*p*)/[2*s*1*p*] valence basis for Cs. For Ge and Br we employed 4- and 7-valence-electron pseudopotentials, respectively, (19) with (4*s*4*p*)/[2*s*2*p*] basis sets (19, 20). We will call this basis-S. (*ii*) For more accurate optimizations of the lattice constant (keeping the other parameters constant for the low-pressure modification) we used a 9-valence-electron pseudopotential and a (5*s*5*p*1*d*)/[3*s*3*p*1*d*] basis for Cs (21), and additional *d*-polarization functions for Ge and Br (denoted basis-L) (22).

We have first carried out molecular test calculations for $CsGeBr_3$ (in C_{3v} symmetry), using the Gaussian92 program (23), to evaluate systematic Hartree–Fock, basis set, and pseudopotential errors, which are expected in the crystal calculations. Calculations including electron correlation at the second-order perturbation theory level (MP2/basis-V) used the same pseudopotentials as the basis-L combination, but an even larger (7*s*7*p*3*d*1*f*)/[6*s*6*p*3*d*1*f*] Cs valence basis. Table 5 lists the results of these calculations. The largest errors occur for the Cs–Ge distance, which is calculated to be larger by ca. 4–5% at the HF level with respect to the more accurate MP2 results. This is due to the well-known importance of core-valence electron correlation for the very polarizable Cs^+ cation. An additional 2–3% error in the Cs–Ge distance is observed upon going from HF/basis-L to HF/basis-S. Errors in the Ge–Br distances are expected to be small at the basis-L level, but become significant (ca. 3%) at the basis-S level, largely due to the neglect of *d*-functions on these two elements.

To estimate the accuracy expected for angular changes in the coordination environment of the germanium atom, we have calculated the planarization barrier for the $GeBr_3$ unit in molecular $CsGeBr_3$ (see Table 5). Apparently, basis set and correlation errors tend to cancel partially at the HF/basis-S level, leading to reasonable agreement with the MP2/basis-V results. But even at the basis-L level, the deviation from the MP2 results is less than 20%. Hence, we expect reasonable HF deformation energies for the much smaller coordination changes in the crystalline environment.

Computational results for the structural parameters and relative energies of $CsGeBr_3$ in the space groups *R3m* and $Pm\bar{3}m$ (using the two different pseudopotential/basis set combinations; see above) are shown in Table 6. Consistent with the molecular test calculations, the Hartree–Fock calculations yield a lattice constant which is

TABLE 5
Results of Molecular Test Calculations for $CsGeBr_3$

Parameter	HF/basis-S	HF/basis-L	HF/basis-V	MP2/basis-V
d(Cs–Ge) (pm)	376.3	367.1	366.9	350.9
d(Ge–Br) (pm)	253.8	247.5	247.3	247.0
Angle Br–Ge–Br' (°)	115.8	116.4	116.6	116.8
E_{plan} (kJ/mole)[a]	74.3	98.8		83.7

[a] Barrier for planarization of the $GeBr_3$ unit.

considerably too large (ca. 7% at the basis-S level, ca. 6% at the basis-L level, see Table 6) mainly due to neglect of core-valence correlation for the Cs atom. Consequently, the deviations for the distances d(Cs–Br) are particularly large. The errors for the distances d(Ge–Br) are also larger than in molecular calculations, due to coupling of the distances d(Ge–Br) with d(Cs–Ge) and d(Cs–Br) in the crystal structure. The positional parameters for calculations in space group $R3m$ are in reasonable agreement with the experimental result even at basis-S level.

The difference between the lattice constants optimized in space group $R3m$ and $Pm\bar{3}m$ (15 pm and 12 pm at the basis-S and basis-L level, respectively) is in good agreement with the compression needed experimentally to induce the phase transition (14 pm). Thus, the structural changes related to the pressure-induced phase transition are simulated quite well by the calculations.

The energy differences given in the last column of Table 6 suggest that the actual energy needed to induce the phase transition is roughly in the 5 kJ/mole range. The energy difference between the $Pm\bar{3}m$ single point calculations at the $R3m$ optimized lattice constants and the fully $R3m$ optimized structures differ too much for the two basis set levels employed to give a reliable estimate for the barrier involved in the thermal phase transition.

DISCUSSION

The distortion of the $GeBr_{6/2}$ octahedra in the crystal structure of the low-pressure modification is attributed to the stereochemical activity of the Ge(II) lone pair (7). The pressure-induced changes of the low-pressure structure are mainly caused by positional shifts of the germanium and bromine atoms. These shifts result in an increase in d(Ge–Br) from 253.4(3) to 257(1) pm and a decrease in d'(Ge–Br) from 311.6(4) to 295(1) pm. As a result the differences $\Delta d = d$(Ge–Br) $- d$(Ge–Br') are reduced from 58.2(4) (ambient conditions) to 38(1) pm (0.8 GPa) corresponding to an increase in the ratio $q = d$(Ge–Br)/d'(Ge–Br) from 0.813 at 0.1 MPa to 0.871 at 0.8 GPa. The bond angle β(Br–Ge–Br) decreases slightly from 95.14° to 94.1°. Thus, increasing pressure to 0.8 GPa changes the deviation of the trigonal antiprismatic coordination from an octahedral arrangement by 30% in q and 20% in β. Parallel to the changes in bond length and angles the deviation of the rhombohedral angle α from 90° is reduced by about 40%, but this decrease has nearly no effect on d(Ge–Br) and d'(Ge–Br). Furthermore, the influence of the rhombohedral angle α on the bond angle β is partly compensated for by positional shifts. As a result, the characteristic Ge(II) lone pair configuration is not essentially changed within the stability range of the low-pressure polymorph.

The negative pressure shift of Raman modes of the low-pressure modification can be explained qualitatively in terms of the continuous structural changes. The strong negative pressure shifts of stretching modes indicate a decrease in the dominant Ge–Br stretching force constant (24). This finding is consistent with the observed increase in the bond length d(Ge–Br) with pressure.

The high-pressure modification of $CsGeBr_3$ shows no first-order Raman effect and is unambigously cubic. Thus, we conclude that the crystal structure of the high-pressure polymorph is that of perovskite with regular $GeBr_{6/2}$ octahedra. In this respect the high-pressure and the high-temperature modifications are different: The structural changes induced by pressure alter the symmetry of the Ge(II) coordination whereas thermal activation preserves the local symmetry of Ge(II).

The structural phase transition at 1.0 GPa is of first order, as indicated by the hysteresis of Raman spectra.

TABLE 6
Calculated (Crystal Hartree–Fock) and Experimental Parameters for the Crystal Structures of $CsGeBr_3$

Soruce	a (pm)	α (°)	x (Ge)	x (Br)	z (Br)	E_{rel} (kJ/mole)[a]
Exp. $R3m$[b]	563.5(9)	88.74(4)	0.4764(4)	0.5018(4)	0.0271(4)	
Exp. $Pm\bar{3}m$[c]		90	½	½	0	
Basis-S, $R3m$ opt.	603.5	90	0.4843	0.5027	0.0271	0
	603.5[d]					+9.6
Basis-S, $Pm\bar{3}m$ opt.	589.0					+4.7
Basis-L, $R3m$[e] opt.	591.6	—	—	—	—	0
Basis-L, $Pm\bar{3}m$	591.6[d]					+28.4
Basis-L, $Pm\bar{3}$ opt.	579.4					+4.3

[a] Energy relative to the $R3m$ minimum at the same theoretical level.
[b] Low-pressure modification.
[c] Crystal structure at a pressure slightly above phase transition.
[d] $Pm\bar{3}m$ single point calculation at $R3m$ optimized lattice constant.
[e] Lattice constant optimized with structural parameters kept at basis-S values.

The change in the rhombohedral angle α from 89.35(3)° to 90° occurs in an interval of less than 0.15 GPa. The magnitude of the observed angle alteration in a small pressure range is compatible with a discontinuous change. Nevertheless, continuous structural changes which are similar to atomic shifts occurring in the induction period of λ-transitions precede the phase transition. Application of the Landau theory reveals that the requirements of a second-order phase transition are fullfilled (25, 26). The fact that there is a continuous transformation path evidences the close structural relationship of the low- and high-pressure polymorphs.

In conclusion, the high-pressure phase transition of $CsGeBr_3$ is an example of a pressure-driven conversion of the Ge(II) electron configuration from a stereochemically active lone pair $n(sp^3)^2$ to an inert electron pair ns^2. It would be interesting to see how this picture is reflected in the valence electron density obtained from band structure calculations for $CsGeBr_3$ at reduced volumes. Further work on the isotypic compounds $CsGeCl_3$ and $CsGeI_3$ is in progress, as well as calculations of the valence electron density and the electron localization function from the band structure.

REFERENCES

1. H. Bärnighausen, *Acta Crystallogr. Sect A* **31,** S3 (1975).
2. H. Bärnighausen, *Math. Chem.* **9,** 139 (1980).
3. J. M. Buerger, *Fortschr. Mineral.* **39,** 9 (1961).
4. K. Gesi, *Phase Transitions* **40,** 187 (1992).
5. A. N. Christensen and S. E. Rasmussen, *Acta Chem. Scand.* **19,** 421 (1965).
6. G. Thiele, H. W. Rotter, and K. D. Schmidt, "Unkonventionelle Wechselwirkungen in der Chemie metallischer Elemente" (B. Krebs Ed.), p. 316. Verlag Chemie, Weinheim, 1992.
7. G. Thiele, H. W. Rotter, and K. D. Schmidt, *Z. Anorg. Allg. Chem.* **545,** 148 (1987).
8. J. Galy, G. Meunier, St. Andersson, and A. Åström, *J. Solid State Chem.* **13,** 142 (1975).
9. A. Neuhaus, *Chimia* **18,** 93 (1964).
10. G. J. Piermarini, S. Block, J. D. Barnett, and R. A. Forman, *J. Appl. Phys.* **46,** 2774 (1975).
11. L. Merril and W. A. Bassett, *Rev. Sci. Instrum.* **45,** 290 (1974).
12. B. Serr, *Thesis, Universität Freiburg,* 1993.
13. J. Weidlein, "Schwungungsspektroskopie," p. 103. Thieme, Stuttgart, 1982.
14. K. F. Tebbe, "Program AGL." Köln.
15. G. Sheldrick, "Program SHELX76." Cambridge, 1976.
16. Further details of the crystal structure analyses may be obtained from Fachinformationszentrum Karlsruhe, D-76344 Eggenstein-Leopoldshafen by quoting the registry No. CSD 62347, the names of the authors, and the journal citation.
17. R. Dovesi *et al.*, "Crystal 92 Program" 1992. For a general description, cf. C. Pisani, R. Dovesi, and C. Roetti, "Hartree-Fock *ab Initio* Treatment of Crystalline Systems, Lecture Notes in Chemistry." Springer, Berlin, 1988.
18. P. Fuentealba, H. Preuss, H. Stoll, and L. v. Szentpály, *Chem. Phys. Lett.* **89,** 418 (1982).
19. A. Bergner, M. Dolg, W. Küchle, H. Stoll, and H. Preuss, *Mol. Phys.,* **80,** 1431 (1993).
20. M. Kaupp, P. v. R. Schleyer, H. Stoll, and H. Preuss, *J. Am. Chem. Soc.* **113,** 6012 (1991).
21. W. Küchle, A. Bergner, M. Dolg, H. Stoll, and H. Preuss, unpublished data.
22. S. Huzinaga (Ed.), "Gaussian Basis Sets for Molecular Calculations." Elsevier, New York, 1984.
23. M. J. Frisch, G. W. Trucks, M. Head-Gordon, P. M. W. Gill, M. W. Wong, J. B. Foresman, B. G. Johnson, H. B. Schlegel, M. A. Robb, E. S. Replogle, R. Gompertz, J. L. Andres, K. Raghavachari, J. S. Binkley, C. Gonzales, R. L. Martin, D. I. Fox, D. J. DeFrees, J. Baker, J. P. Stewart, and J. A. Pople, "Gaussian 92, Revision A." Gaussian, Inc., Pittsburgh, PA, 1992.
24. H. Tanino, M. Holtz, M. Hanfland, K. Syassen, and K. Takahashi, *Phys. Rev B* **39,** 9992 (1989).
25. V. L. Indenbom, *Kristallografiya* **5,** 115 (1960); *Sov. Phys. Crystallogr. Engl. Trans.* **5,** 106 (1960).
26. C. Haas, *Phys. Rev. A.* **140,** 863 (1965).